JOURNAL OF MATERIALS SCIENCE 29 (1994) 6551–6560

Kinetic microhardness measurements of sialon-based ceramics

A. L. YURKOV, N. V. JHURAVLEVA, E. S. LUKIN
Department of Ceramics, Mendeleev University of Chemical Technology of Russia, Moscow, 125190, Russia

The conventional procedure of microhardness testing consists in applying a fixed load on an indentor and measuring the square of the indent under the microscope. The method of kinetic microhardness (registration of the depth of penetration of an indentor as a function of load) reveals new features of mechanical characteristics of the surface of brittle materials. The investigated sialon-based ceramics demonstrate unrelaxed hardness from 5–13 GPa and elastic relaxation up to 60%–63%. Analysis of the surface layers was made in ranks of the Meyer's equation. The value of the coefficient, N (Meyer's index), of the best investigated materials was found to be 2, varying from 0.92–2.10.

1. Introduction

The conventional procedure of microhardness testing consists in applying a fixed load on a diamond indentor and measuring, with the help of a microscope, the square of the indent on the surface of the tested material after unloading.

The registration of the depth of penetration of the indentor in the material as a function of load allows determination of the deformation of the material under an indentor at increasing and fixed load, and the relaxation of the material during unloading. The kinetic microhardness method has been in use from the 60s; a major work was carried out on metals and alloys by Bulyichev and Alekhin [1].

Microhardness, as a technological characteristic of materials, is used universally. Indentation tests to measure fracture toughness of materials, following Evans and Charles [2] and many other researches [3–5] are accepted worldwide. Studies of fracture toughness by indentation are continuing. However, investigation of other characteristics of materials, related to hardness, are limited by the precision of the equipment used.

A contact microhardness tester (a device for kinetic microhardness measurement) opens a way to investigate conventional characteristics in more detail, with the help of the standard indentation testing procedure. It may also advance the research of new characteristics of a material, which may be obtained by analysis of indentation data. Some work using a device of this type has been carried out on MgO and Al_2O_3 [6].

The indentor progressively penetrates the material, as the load on the indentor monotonically increases up to a maximum load. Then the load on indentor gently decreases, and the indentor moves away, as the material relaxes. The load and depth of penetration of the indentor are registered on an X–Y recorder. A typical load–depth of penetration of indentor plot is shown in Fig. 1, which shows the loading curve, OA, and the unloading curve, AC. The trace of the penetration of the indentor at fixed load (not shown) is a horizontal step, beginning from point A. Plots of microhardness versus depth of penetration, or microhardness versus load are easily available from load–depth of penetration plots. Other characteristics will be discussed in the text.

2. Experimental procedure

2.1. Preparation of samples

The investigated materials were sialon-based ceramics of the system Y–Si–Al–O–N (Table I). The starting materials were Si_3N_4, AlN, Al_2O_3 and Y_2O_3. Silicon nitride powder, with a specific surface area of 25–30 $m^2\,g^{-1}$, was prepared by plasmochemical synthesis (chemical composition N > 37.0%, free Si < 1.0%, O < 2.0%, Al < 0.2%, Fe < 0.1%, Ca < 0.01%). Oxides and AlN also were prepared by plasmochemical synthesis and had specific surface areas of 15–18 $m^2\,g^{-1}$.

The powders were mixed in a planetary mill in teflon drums in acetone. After mixing, the powders were dried, disintegrated and cold isostatically pressed without binders at a pressure of 1000 MPa. The samples were sintered according to two-step regime. During the first cycle, the samples were sintered at 1800 °C and 1.5 MPa for 15 min up to zero accessible porosity. During the second cycle, the pressure was raised to 70 MPa at 1750 °C for 1 h.

2.2. Testing of materials

The samples were diamond-cut and polished. The bending strength of the samples in three-point bending was measured, using 4 mm × 4 mm × 35 mm bars (Table II). The fracture toughness was measured by the indentation technique, using Evans and Charles' method [2] at a load of 98.1 N. The micro-

0022–2461

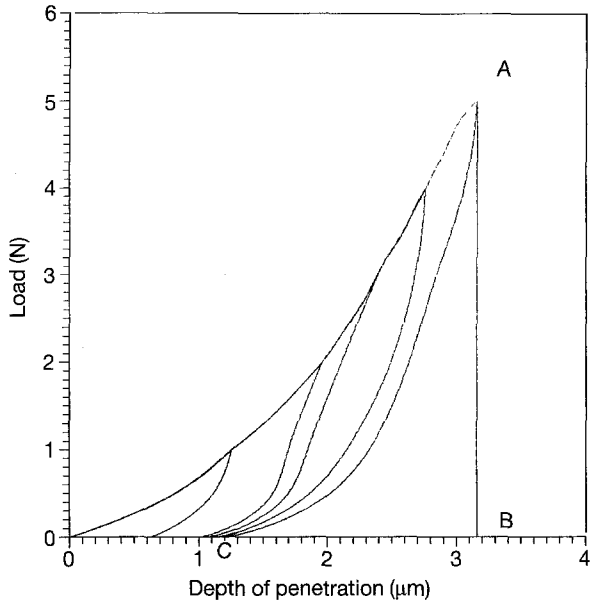

Figure 1 The standard plot of load–depth of penetration of the indentor, obtained with the help of the contact microhardness tester: OA, loading curve; AC, unloading curve (sample N1).

structure of the materials was investigated by scanning electron microscopy and a petrographical microscope. Phase analysis was performed using X-ray diffraction analysis (XRDA) and a petrographical microscope.

The hardness, with the help of a macrohardness tester, was measured at 98.1N.

The principles of the contact microhardness tester are shown in Fig. 2. The carriage (4) carries the loading mechanism, (the rod, 5, with the indentor, 6, hanging on elastic strings, 8), and mechanism for registering the load (9) (a mechanotrone dynamometer), and moves in the direction of the drive mechanism (1). The movement of the carriage (4) is achieved by belt transmission (2) and a microscrew (3) driven by an electric motor (not shown).

A mechanotrone dynamometer was used to analyse elastic deformation in the loading mechanism. The mechanotrone sensor transforms mechanical deformation in the electric signal. The mechanotrone dynamometer is made from a mechanotrone in a heatproof housing and a mechanism of mechanical balance to zero the sensor. The mechanotrone rod with the help of the sensor tip, makes contact with the stop plate of the loading mechanism.

The elastic strings have two roles: firstly, they are the elastic elements, with the help of which the sample is loaded; secondly, they provide the directions for vertical movement of the rod with the indentor. In order to register micromovements, a mechanotrone sensor (10) (mechanotrone micrometer) is used. The body of the sensor (10) is placed on the stationary base of the tester. The measuring bar of the sensor is in contact with the rod.

Before the experiments, there was a clearance between the base of the specimen and the indentor. The mechanotrone dynamometer and micrometer were adjusted so that their output electric signals were zero.

TABLE I Starting powders and compositions of sintered materials

N	Specific surface area ($m^2 g^{-1}$)		Addition (wt %)	Methods of manufacturing	Main phase	Additional phase
	Si_3N_4	Additions				
1	25–30	15–18	5% Y_2O_3 2% Al_2O_3 3% AlN	sintering 2 MPa N_2 + HIP	β′-sialon $Z = 0.35$	Glassy phase
2	25–30	15–18	3% Y_2O_3 4% Al_2O_3 14% AlN		β′-sialon	Glassy phase, 12H
3	25–30	15–18	6% Y_2O_3 4% Al_2O_3 10% AlN		β′-sialon α′-sialon β′: α′ = 9:1	Glassy phase, 12H
4	25–30	15–18	3% Y_2O_3 4% Al_2O_3 10% AlN		β′-sialon α′-sialon β′: α′ = 8:2	Glassy phase
5	25–30	15–18	3% Y_2O_3 8% Al_2O_3 8% AlN		β′-sialon	Glassy phase

TABLE II Characteristics of sintered materials

N	Apparent porosity (%)	Density ($g cm^{-3}$)	Bending strength (MPa)	K_{IC} ($MPa m^{1/2}$)	H_v(98.1 N)(GPa)
1	< 1	3.19	650 ± 50	5.5 ± 1.3	19.2 ± 1
2	< 1	3.22	450 ± 50	5.1 ± 1.4	18 ± 1
3	< 1	3.24	450 ± 50	4.8 ± 1.4	19 ± 2
4	< 1	3.22	650 ± 50	5.2 ± 1.5	19 ± 2
5	< 1	3.24	500 ± 50	3.7 ± 1.4	14.4 ± 1

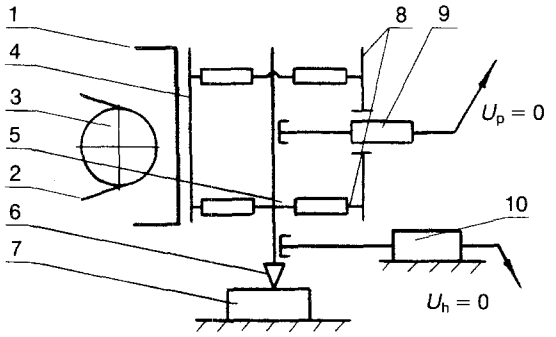

Figure 2 The principal parts of the contact microhardness tester: 1, drive direction; 2, belt transmission; 3, microscrew; 4, carriage; 5, rod; 6, indentor; 7, specimen; 8, elastic strings; 9, mechanotrone dynamometer; 10, mechanotrone sensor.

The output signal of the dynamometer applies input Y of an X–Y recorder (the load). The output signal of the micrometer applies input X of the X–Y recorder (depth of penetration).

The electric motor slowly rotates the microscrew (3), which transmits the movement by a lever-gear drive mechanism to the vertical movement of the carriage. As the carriage descends, the clearance diminishes. At this point, there is no load on the rod with the indentor, and the output signal of the dynamometer is zero. The output signal of the micrometer is proportional to the movement of the rod. As a result, the recorder registers the horizontal line along the X coordinate.

At the moment the indentor contacts the specimen with the subsequent movement of the carriage, the strings (8) are deflected. This deflection, proportional to load, P, is registered by the dynamometer (9). The recorder begins to trace the diagram (Fig. 1), beginning from point O. The electric motor switches off at maximum load, P_A, which is proportional to the maximum deflection of the strings. The sensor registers the maximum depth of penetration, h_B. The electric motor reverses, and the carriage lifts. As the action of the strings diminishes, the load and depth of penetration also diminish (elastic recovery). After unloading, the carriage returns to its starting point.

The accuracy with which the depth of penetration of the Vickers diamond indentor is recorded, is 0.02 μm (taking into account time-dependent flow of the electric current of the sensor during intrusion of the indentor). The accuracy of measurement of the load was 0.05 N. The rate of penetration of the indentor into the material was about 0.3 mm s^{-1}.

The value of unrelaxed microhardness, H_v, is calculated as

$$H_v = 0.037\,84\frac{P}{h^2}, \qquad (1)$$

where P is the load (N), and h the unrelaxed depth of penetration (μm).

The plot of load against depth of penetration is easily converted to a plot of microhardness against load (Fig. 3a) or microhardness against depth of penetration (Fig. 3b). The load–depth of penetration plot may also be converted to a logarithmic plot, log$P$–log$h$ (Fig. 4).

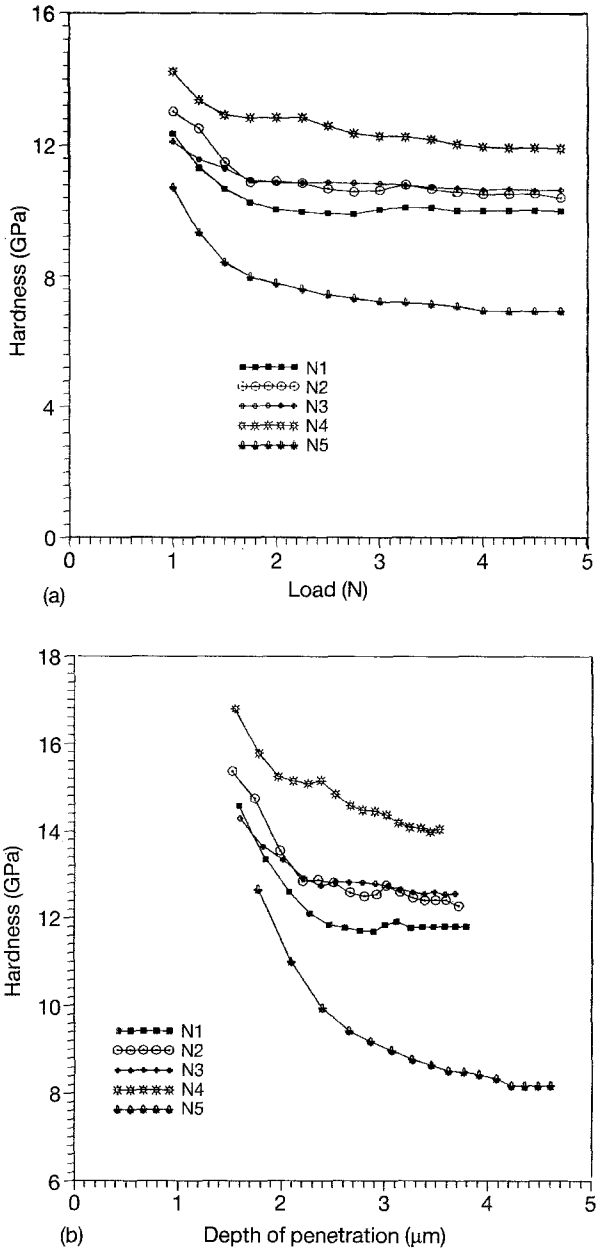

Figure 3 Plots of (a) hardness–load and (b) hardness–depth of penetration.

The indentation cycle was repeated at ten points on each specimen with a distance of 0.5 mm from one indentation point to another. The individual plots of microhardness against load (or depth of penetration), are not monotonic and vary from one point of indentation to another (Fig. 5a, b). The deviation of microhardness values of the materials is characterized with the help of a coefficient of variation

$$c = D/m \qquad (2)$$

where D is the variance in values of microhardness from ten points at fixed load, and m is the average value. The coefficient of variation–load (or depth of penetration) plots are not monotonic (Fig. 6).

The square of the curve OABO (Fig. 1) is the work of intrusion of the indentor, or the work of deformation of the material, and may be calculated from

$$Ad = \int_0^{h_{max}} P\,dh = S_{OABO} \qquad (3)$$

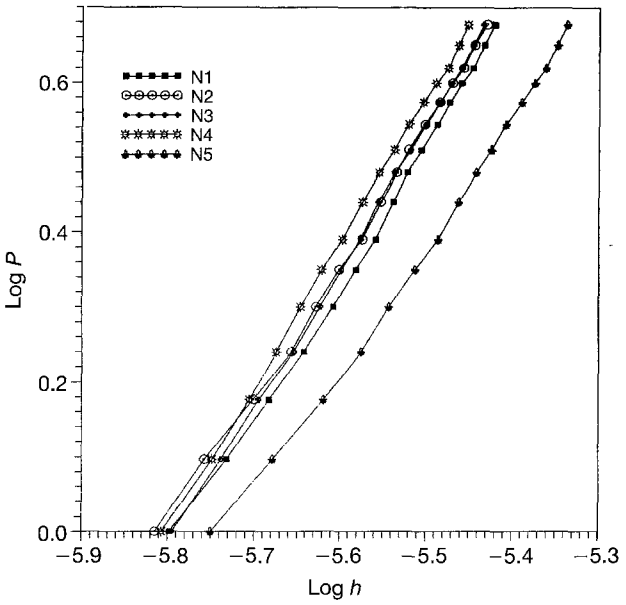

Figure 4 Logarithmic plots of load–depth of penetration.

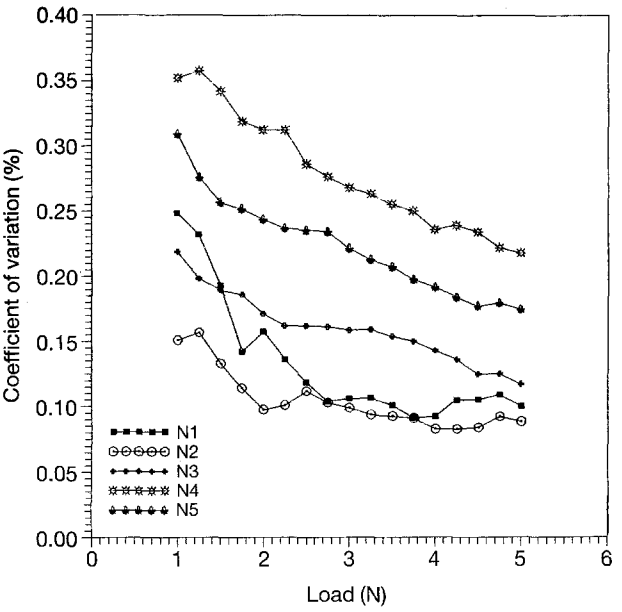

Figure 6 Plots of coefficient of variation of values of the microhardness versus load.

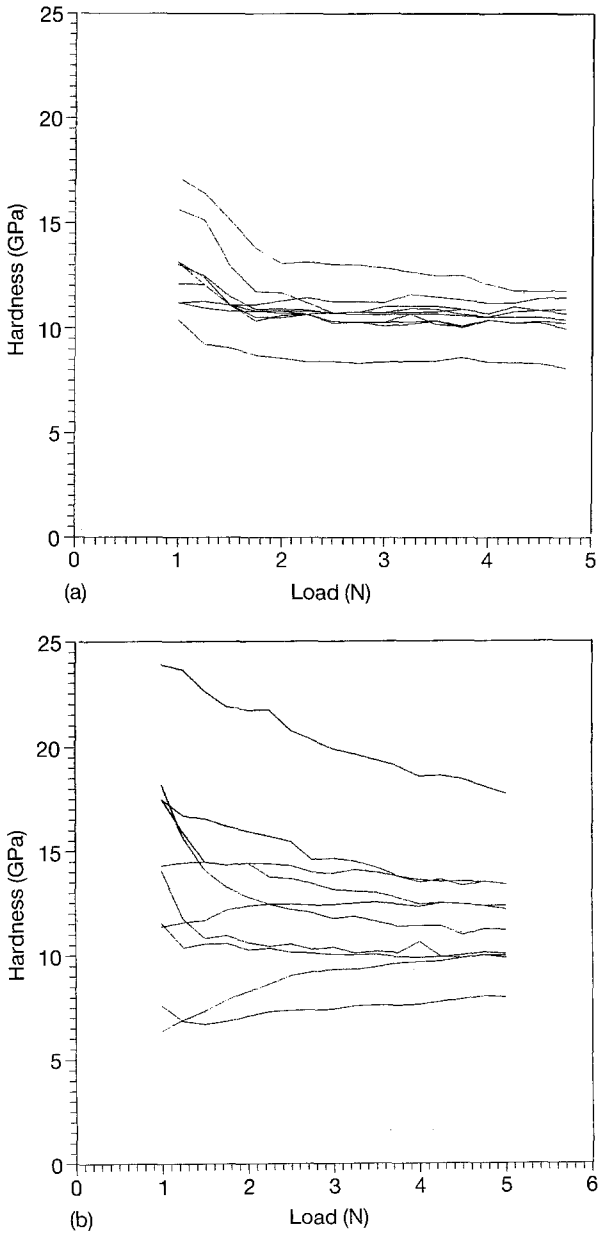

Figure 5 Individual plots of hardness–load, obtained from ten points on (a) sample N1 and (b) sample N4.

The work of deformation of the material is the sum of the work of plastic deformation

$$Apd = S_{OACO} \quad (4)$$

and the work of relaxation

$$Ar = S_{CABC} \quad (5)$$

The ratio of the work of relaxation to the work of deformation is the coefficient of relaxation

$$\alpha r = Ar/Ad \quad (6)$$

Plots of the work of deformation, work of plastic deformation, work of relaxation, and coefficient of relaxation, against load, may be obtained by varying the maximum load, as shown in Figs 1 and 6a–d.

After unloading it is possible to measure the length of the indent diagonal under the microscope (a conventional procedure) and to calculate the relaxed microhardness according to

$$H_v = 0.4636\frac{P}{a^2} \quad (7)$$

where a is the length of the half-diagonal of the indent. The relaxed microhardness, calculated in such a way, is always greater than the value of unrelaxed microhardness. Relaxation of the indented area takes place, and the depth of penetration, calculated according to geometry from the relaxed half-diagonal of the indent, is always lower. This comparison of relaxed and unrelaxed microhardness may also be a characteristic of the material.

3. Results and discussion

3.1. Characterization of the samples

The materials were dense (porosity < 1%). The structure of sample N1 consists of needle-like crystals (d = 1–2 μm, l = 15–50 μm, sometimes reaching 70 μm) and isometric grains (Fig. 8a). The needle-like

crystals form a framework inside which round-shaped grains occur. The glassy phase forms interlayers between the isometric grains.

According to SEM (Fig. 8b–e), the microstructures of samples N2, N3, N4 and N5 are very much alike. The grains are isometric or short prismatic (d = 1–2 μm, l/d = 2). The glassy phase is in form of continuous and discontinuous layers between the grains and has a refraction index of 1.6. According to XRDA samples, N1, N2 and N5 are β′ sialon compositions (Table I); in sample N3 the β′:α′ sialon ratio is 9:1, in sample N4 it is 8:1.

The mechanical characteristics of the materials do not differ greatly. The maximum bending strength, 650 MPa, is reached in samples N1 and N4. The same materials exhibit the greatest values of relaxed hardness and considerable fracture toughness. The ratio of maximum to minimum value of bending strength, hardness and fracture toughness is 1.3–1.5.

Taking into account the mentioned conventional mechanical characteristics, we may suppose that the best materials for structural application (especially wear application) may be N1 and N4.

3.2. Kinetic microhardness characterization of materials

3.2.1. Hardness–load and hardness–depth of penetration dependences, and coefficient of variation

Kinetic microhardness data show complex dependencies. The ratio of maximum to minimum value of unrelaxed microhardness is 1.2 at 1N load, and 1.85 at 5N load (Fig. 3a). The range of values is wider than the range of conventional characteristics.

Sample N4, the composition with α′:β′ = 20:80, has hardness values 13.7 GPa at 1N load and 13 GPa at 5N load. Sample N5 (β′ composition) at 1N exhibits a hardness of 11 GPa and at 5N, 7 GPa.

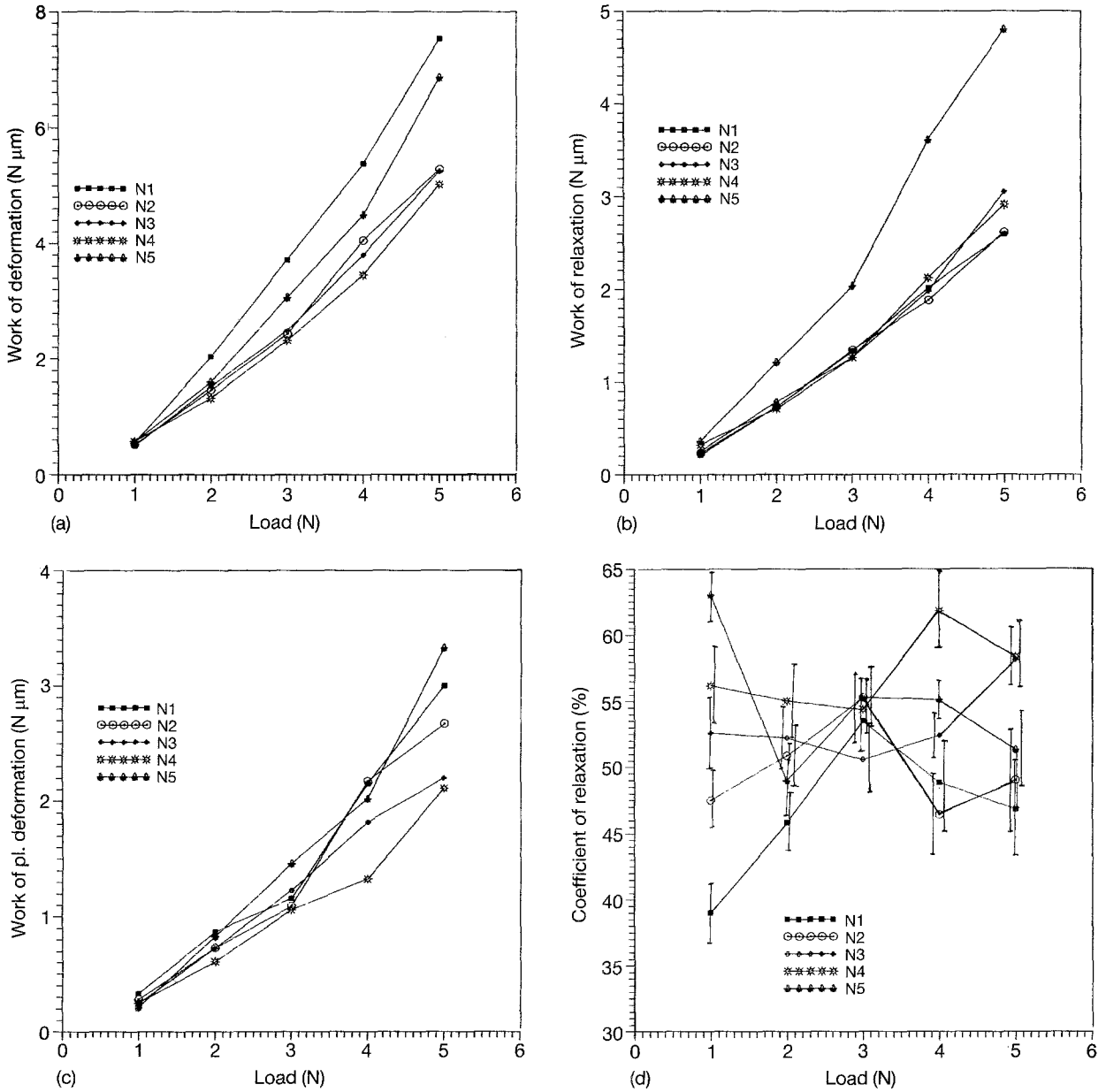

Figure 7 Plots of (a) work of deformation, (b) work of relaxation, (c) work of plastic deformation and (d) coefficient of relaxation, during indentation versus load.

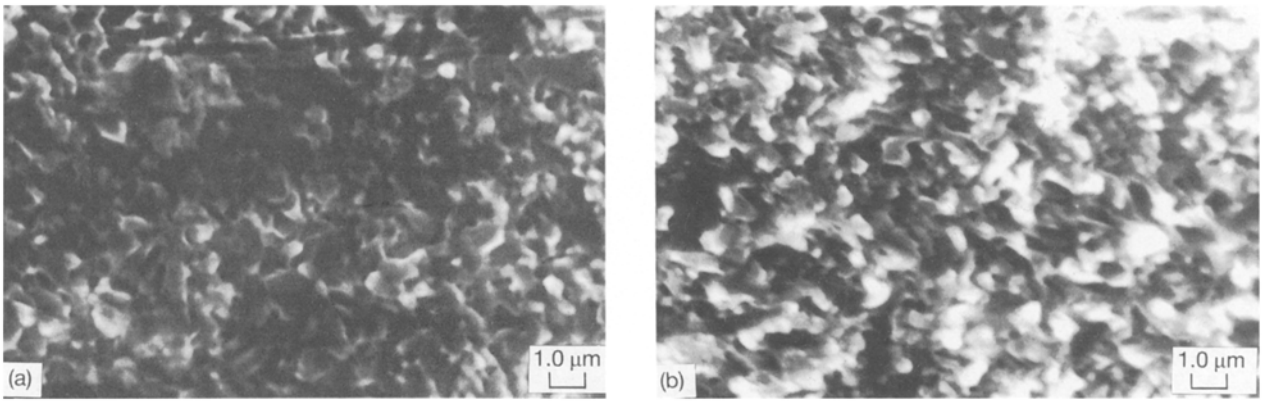

Figure 8 Structure of (a) sample N2 and (b) sample N4.

The accuracy of the equipment provides additional information about the spread in values of microhardness. An individual plot of microhardness against load may not be monotonic (Fig. 5a, b), having steps and inflection points. Ten dependencies, measured on one sample, can be averaged. There are two possible ways to depict the spread of microhardness values: with the help of a plot of the confidence level of values of microhardness versus load, or with the help of the coefficient of variation. The plot of confidence level of microhardness values (Fig. 9) is more instructive, but it is difficult to depict a set of dependencies of this type on one figure. The plots of coefficient of variation (Fig. 6) are not monotonic and characterize inhomogeneity of the materials. The coefficient of variation is a "technological" characteristic of a material.

The best materials from the view point of the coefficient of variation are N1 and N2. The materials with the greatest deviation are N4 and N5. The hardest material, N4, shows the greatest deviation in microhardness values over all intervals, which is manifested in the microstrained structure.

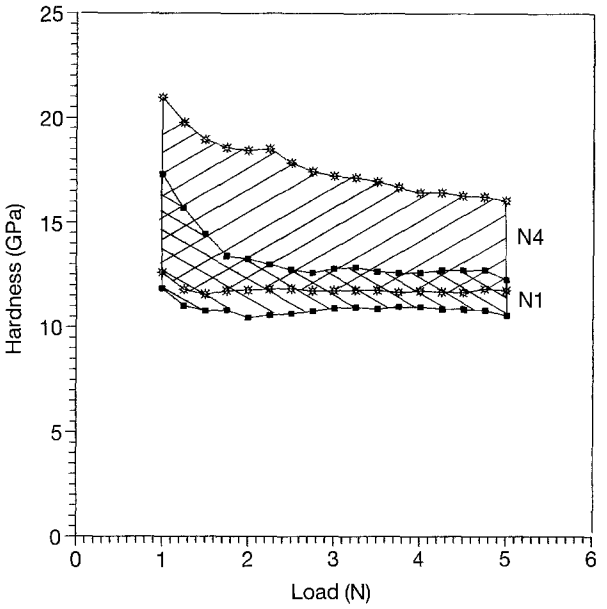

Figure 9 The plots of the confidence level of values of microhardness versus load of samples N1 and N4.

3.2.2. Indentation size effect

The hardness should be independent of the size of the indent, because the pressure used to produce the indent of proper size is a measure of hardness (Equation 1). Therefore, when the hardness increases, as the applied load decreases (Fig. 3a, b), it must be because the volume of material used to yield is smaller, and the mechanism for yielding is dependent on the volume, which becomes more significant as the indent size decreases.

The load dependence of hardness is called the indentation size effect (ISE). Bulyichev and Alekhin [1] termed this phenomenon the scale indentation effect.

The load dependence of the diagonal size of the indent can be modelled by a power law

$$P = KD^n \tag{8}$$

where P is the load, K a constant and D the length of the indent diagonal. Equation 8 can be rewritten in the form

$$P = ah^n \tag{9}$$

where a is the transformed constant, and h is the depth of penetration of the indentor.

Equation 8 or 9 is called Meyer's law or the log-index relationship. The value of Meyer's index, n, is used as a measure of ISE. If the hardness is independent of load, n must equal 2. If the hardness increases when the applied load decreases, $n < 2$. If the hardness decreases when the applied load decreases, $n > 2$. Deviations from $n = 2$ are a measure of ISE and for a certain material in a specific case will be a measure of microstructural variations, surface layers, mechanochemical effects, etc.

The coefficient a has a value of load that is required to produce an indent at a depth of 1 μm (Equation 9), and so this parameter is connected with the strength of the material. In addition, the hardness at a depth 1 μm (Equation 9), is somehow connected with the theoretical hardness of the material, and can only be used for comparison of materials.

It is possible to substitute Equation 9 into Equation 1

$$H = 0.3784\frac{P}{h^2} = 0.3784\frac{ah^n}{h^2} = 0.3784\,ah^{n-2} = 0.3784\,a[(P/a)^{1/n}]^{n-2} = 0.3784\,a(P/a)^{(n-2)/n} \quad (10)$$

The next modification gives

$$H = 0.3784\,a^{2/n}P^{(n-2)/n} \quad (11)$$

indicating that hardness is dependent on load and n in all cases if $n \neq 2$.

The general reasons for ISE are that the shallow near-surface volume of the deformation zone can become a significant fraction of the total affected volume, when a small load on the indentor is used. Thus, the work-hardening layers, surface-compressed layers, ion-implanted layers and possibilities for chemical reactions between the atmosphere and the surface, can dominate the yielding mechanism to produce non-standard hardness values. Conversely, these phenomena could be studied by measuring ISE.

In order to make an analysis, Equation 9 may be written as

$$\log P = \log a + n\log h \quad (12)$$

Thus corresponding values of log$P$ and log$h$ are plotted and a straight line is fitted to the data obtained, from the slope of which n can be found (Fig. 8).

Equal values of hardness at definite load and different values of n for two materials suggest different abilities to deform. If the indent occupies a considerable number of grains, the ability to deform must be independent of load and $n \Rightarrow 2$. The explanation assumes, that $n = 2$ in an averaged result, which can be reached with increasing number of grains.

Accurate measurements provide data that cannot be approximated as a straight line in log$P$–log$h$ (or log$d$) coordinates. Buckle [7] revealed this fact, working with copper and copper–titanium alloys. He suggested that indentations made at very small loads approach the conditions of single-crystal microhardness, so that corresponding hardness values tends to satisfy $n = 2$. On the other hand, the hardness values obtained at high loads, reflect a behaviour of quasi-homogeneous structure and tend to satisfy another straight line with $n = 2$. Hence, the hardness curve, established in the range of loads, passes from one basic form to another, and tends to have a complex form (Fig. 10).

Sargent and Page [8] worked with MgO ceramics, having average grain sizes of 12.9, 30.4 and 102.8 μm. They obtained reliable but different values of Meyer's index from plots of ln P–ln d in the transition zone and values of $n = 2$ exterior to the transition zone.

In our research, all plots of log$P$–log$h$ (Fig. 4) have one, two, three or four points of inflection. The region

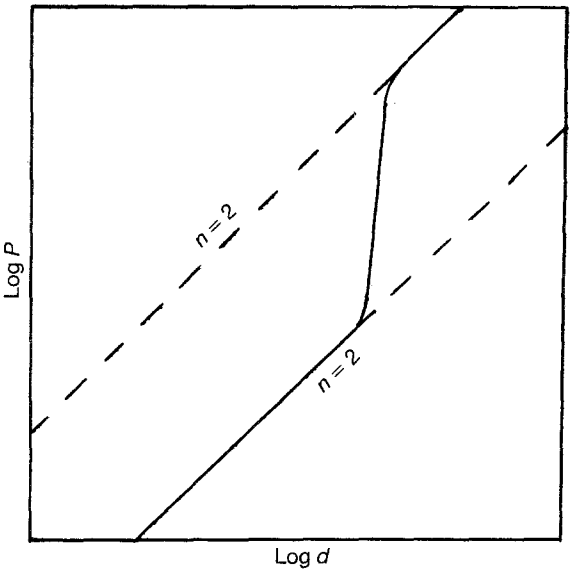

Figure 10 Logarithmic plot of load–half diagonal of indent, after Buckle [7].

between the first and the second inflection points may be interpreted as a transition zone. This type of behaviour takes place in sample N4. After the transition zone, the values of a and n change.

The inflection takes place at a depth from 1.56–3.72 μm, which corresponds for Vickers indentor to a diagonal from 10.5–25.9 μm. In the case of sample N2, the inflection point is at a depth of 2.34 μm, which corresponds to a diagonal of 16.5 μm. The structure of sample N2 consists of grains 1–3 μm in size. Thus, before the first inflection point, a volume of 5–10 grains has one slope n and value a, but when the yielded volume grows a little, the law of deformation changes.

We presume that, although the facts described by Buckle, Sargent and Page may take place, the picture is more complicated. It is possible to make a more accurate determination of coefficients n and a from Equation 12.

$$\int_{P_2}^{P_1} \mathrm{d}\log P = \log a + \int_{h_2}^{h_1} \mathrm{d}\log h \quad (13$$

$$\log P_i\Big|_{P_2}^{P_1} = \log a_i + n\log h_i\Big|_{h_2}^{h_1} \quad (14)$$

The solution of linear equation gives a set of values of n and a. (A plot n versus depth of penetration is shown in Fig. 11.)

There is another approach to determine the coefficient n [11]. It is possible to rationalize Equation 12 by differentiation, which then provides the ability to find coefficient n at any point of a curve.

$$\mathrm{d}H = ea(n-2)h^{n-3}\mathrm{d}h \quad (15)$$

Normalization of hardness allows elimination of coefficients a and c

$$\frac{\mathrm{d}H}{H} = \frac{ca(n-2)h^{n-3}\mathrm{d}h}{cah^{n-2}} \quad (16)$$

$$\frac{\mathrm{d}H}{H} = \frac{(n-2)\mathrm{d}h}{h} \quad (17)$$

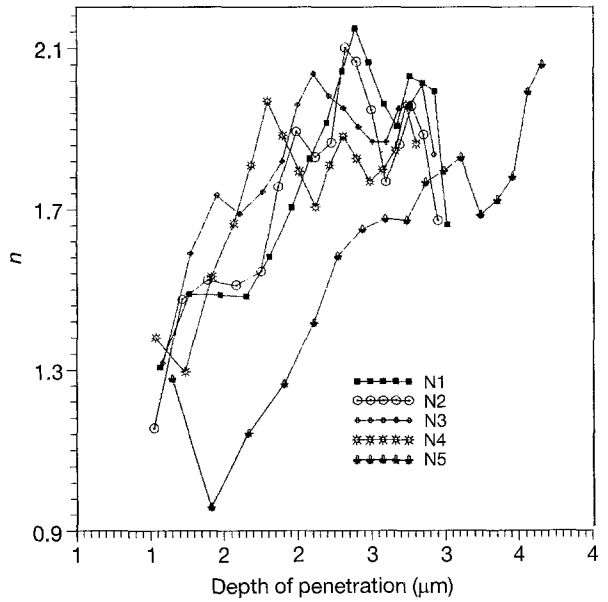

Figure 11 Values of Meyer's index n, versus depth of penetration of the indentor from "dif–log" analysis.

Equation 14 integrates to the following expression at a condition where n = constant

$$\ln(H_1/H_2) = (n-2)\ln(h_1/h_2) \quad (18)$$

So, the combination of Meyer's conventional power analysis with differentiation gives the expression

$$n = \frac{\ln(H_1/H_2)}{\ln(h_1/h_2)} + 2 \quad (19)$$

It is now possible to see (Fig. 11) that the coefficient n is not constant. Equation 12 may be approximated as a line in a very narrow interval.

"Dif–log" analysis is more instructive (it may be fulfilled using values of relaxed and unrelaxed hardness). The inflections on log–log plots coincide with inflections on the "dif–log" plots. One of the features of the n–h plot is extreme. On a plot of sample N1, n increases linearly from 1.45 to 2.15. Thus, the ability to deform diminishes with increasing load (compressed grain or layer under indentor). Then n diminishes to 1.8 and begins to grow again. The behaviour of other samples is similar.

The inflections at a load of 1.25 N or near this load are not so significant, as can be seen from the log–log plot. This local extreme really takes place on almost all the curves and may be attributed to the border of the surface layer. This surface layer depends not only on the manufacturing of material, but also the change of method and regime of surface treatment, which may change the characteristics of the surface layer.

All the samples have an ISE effect, the value of which differs from sample to sample. Finally, all samples reach $n \Rightarrow 2$ ($1.8 < n < 2$). In materials N1 and N5, surface layers differ from the inner part of the material (at first the coefficient n is low). The materials have weak surface layers, but a good inner structure. They require additional surface treatment, which may lead to improvement of the surface.

The difference between the surface and the interior material in samples N2, N3 and N4 is low, because ISE is very little effective. Their hardness is almost independent of load. The materials exhibit good bonding between grains and perfect inner structure of grains.

3.2.3. Work of deformation and related characteristics

The work of relaxation and the work of plastic deformation and its balance with the coefficient of relaxation, characterize the elastic and plastic properties of the material. It could be compared with the rigidity of atomic bonds [12]. The increase in rigidity causes an increase in relaxation and a reduction of plastic deformation.

The curves of the coefficient of relaxation are not continuous; maxima and minima occur on the curves of work of deformation, work of plastic deformation and work of relaxation. There are only five points on each curve (each point is ten indentations). The real form of the curves is unknown. We can only suppose that the extreme of the plot of coefficient of relaxation of sample N1 is situated in the region of 3N.

The values of work of relaxation for all materials except N5 are very close; the work of relaxation of sample N5 is much greater, compared with the other materials over the entire loading interval. The minimum value of the work of plastic deformation is found in the hardest material, N4. The value of the work of plastic deformation of the "softest" material, N5, is rather high (in comparison with the other samples). Therefore, the coefficient of relaxation of sample N5 is "moderate".

Samples N1 and N2 show a tendency for relaxation to increase up to 55% at 3N, then the relaxation falls. The behaviour of sample N4 (the hardest composition with α':β' = 20:80) is similar – relaxation increases up to 62% at 4N load, but with increasing load, relaxation falls. Sample N3 did not show any clear tendency and has a relaxation of 52%–57%. Sample N5 has a maximum relaxation of 63% at 1N load, then relaxation falls to 48%–52%. Generally, there is a correlation between relaxation and hardness.

3.2.4. General characterization of the investigated samples

Additional characteristics of mechanical properties of the surface of sialon-based materials requires accurate interpretation, but opens the way to forecast engineering applications.

Material N5 has the lowest value of hardness, the greatest depth of indentor penetration and considerable ISE (coefficient n begins from 0.92 and finally reaches 1.8). Thus, this material has weak surface layers and the sintering process was incomplete. The relaxation of sample N5 is medium. The coefficient of variation is rather high, showing considerable inhomogeneity.

Materials N1, N2, N3 and N4 are hard and their relaxation is considerable. There is a pronounced difference in properties of the surface layers in sample N1: it requires additional treatment.

Materials N2, N3 and N4 have little ISE effect and would not require additional treatment. Material N4

is the hardest sample, but it has the greatest coefficient of variation. The deviations reach 6 GPa. It cannot be recommended for engineering purposes. However, accurate modification of the temperature regime of sintering may lead to a reduction of its inhomogeneity.

Therefore, the best materials are N2 and N3. Material N1 is also good and may be recommended for engineering applications after additional surface treatment.

4. Conclusion

The method of kinetic microhardness reveals additional characteristics of investigated samples which lead to a deeper understanding of the structure of materials.

Materials can be characterized by the dependence of the unrelaxed microhardness on load or depth of penetration of the indentor and coefficient, n, in Meyer's equation, a measure of the indentation size effect.

Sialon-based ceramics demonstrate unrelaxed hardness 7 GPa $< H_V(5N) <$ 13 GPa. In the best materials, the coefficient $n \Rightarrow 2$, having the range $0.92 < n < 2.10$.

Inhomogeneity of materials can be characterized by the coefficient of variation of the microhardness values.

The materials demonstrate elastic relaxation after unloading, the best samples having a relaxation of 60%–63%.

Appendix 1. Attempts to explain the inflections on the plots

Lawn and Swain [12, 13] analysed the nucleation stage of median crack formation. Their analysis highlights the fact that no flaw can extend to initiate the median crack length unless a critical load is exceeded. Therefore, it is possible to estimate critical loads, sufficient to cause the formation of median cracks in brittle solids.

$$P_{crit} = \frac{34.67\, K_c^4}{\phi^2 \Theta^4 H_v^3} \quad \text{(A1)}$$

where $\phi = 1$ and $\Theta = 0.2$, K_c is fracture toughness and H_v is the Vickers hardness.

The model is suitable to estimate the critical loads only by one order of magnitude. However, it gives values of critical loads that correspond to inflection points obtained by log–log and "dif–log" analysis N1 and N2 (Table III).

The ideas of estimating critical load and critical work done to initiate cracking, were first proposed by Palmqvist [14]. The main problem was the accurate experimental determination of critical load.

We have attempted to interpret the inflections of the curves of coefficient of relaxation also as responses to the appearance of the median crack under the indentor. General considerations give a picture in which, after the appearance of a crack, the relaxation should diminish (minimum on the coefficient of relaxation curve). Table III gives the range between points,

TABLE III Critical values of load, calculated from Equation A1, estimated from plots of work of deformation and "dif–log" analysis and fracture toughness, calculated from Equation A1

N	P_{crit} (N) from Eq. A1	P_{crit} (N) from k. rel.	P_{crit} (N) from "dif–log" analysis	K_{IC} (MPa m$^{1/2}$) from Eq. A1
1	2.8	< 3	2.75–3	5.3
2	2.3	$3 < P < 4$	2.4–2.5	5.06
3	1.97	$2 < P < 3$	2.8–3	5.18
4	1.98	< 3	2.1–2.4	5.76
5	1.36	< 2	1.75	3.92

where measurements were made. The agreement of the data from "dif–log" analysis, analysis data of relaxation and critical load, calculated from the measured fracture toughness, does not often occur.

There is no evidence of the existence of median cracks under indentor. Estimations show that crack initiation may occur, yet the estimations are not very strict, and cannot be proof of cracking.

If the idea of cracking is incorrect, it is necessary to suppose the existence of a strengthened layer at a depth of 2–5 μm.

Appendix 2. Statistical estimations

All averaged values and deviations were calculated at a probability of 95% assuming normal distribution. In order to verify this assumption, sample N5 was indented 100 times up to 5N load. The distributions were calculated at loads of 1, 2, 3, 4, and 5 N. According to the χ^2-criterion, the data fit a normal distribution over the entire range of loads. The form of the distribution changes slightly (skewness at 1N is 0.5298 and at 4N is -0.3217, and the kurtosis at 1N is 2.25 and at 4N is 0.8746).

The other problem concerns the reliability of log–log and "dif–log" analysis. The deviation of values of depths of penetration is considerable, and the problem exists of whether the inflections on the log P–log h plots really occur. The other variant is the approximation of the log P–log h plot (Fig. 4) with a linear equation. The equation will give single values of coefficients n and a.

The adequacy of the equation may be tested with the help of Fisher's criterion

$$F = s_{ad}^2/s_{er}^2 \quad \text{(A2)}$$

where s_{ad}^2 is the variance of adequacy and s_{er}^2 is the error mean square variance.

In our research, the number of experiments (the number of indentations on one sample) is the same, and equals 10. The variance of adequacy is therefore

$$s_{ad}^2 = \frac{m \sum_{i=1}^{n} (\bar{y}_i \hat{y}_i)}{n - l} \quad \text{(A3)}$$

where m is the number of experiments, n the number of experimental points in one experiment, l the number of coefficients in the regression equation (Equation 2), $\bar{y}_i$ the averaged value of log$h$ at fixed log P, $\hat{y}_i$ the value

TABLE IV The variance of adequacy, the error mean square variance, its ratio and the standardized quartile of Fisher's distribution

N	s^2_{ad}	s^2_{er}	s^2_{ad}/s^2_{er}	F_{1-p}
1	0.074 39	0.002 48	29.9721	2.2
2	0.123 70	0.001 14	108.3588	2.2
3	0.111 54	0.001 74	64.0752	2.2
4	0.154 89	0.005 63	27.5279	2.2
5	0.008 71	0.003 86	2.2545	2.2

of $\log h_i$ from the linear regression equation.

The error mean square variance is

$$s^2_{er} = \frac{\sum_{i=1}^{n}\sum_{u=1}^{m}(y_{iu} - \bar{y}_i)^2}{n(m-1)} \quad \text{(A4)}$$

where y_{iu} is the real value of $\log h$ for fixed $\log P$ in the only experiment.

Table IV gives the values of variance of adequacy, the error mean square variance, its ratio and quartile of Fisher's distribution for a significance level $p = 0.05$. In all cases, the ratio s^2_{ad}/s^2_{er} is greater than the value of standardized F_{1-p}.

Equation 14 is not adequate to describe the experimental data. The inflections occuring on $\log P$–$\log h$ plots and "dif–log" analysis is significant.

The only case when the ratio s^2_{ad}/s^2_{er} is close to F_{1-p} (but not lower) is for sample N5. The deviation of the values of depth of penetration is considerable, and the change in coefficient n is not great. This plot should be approximated with two linear equations.

Acknowledgements

The authors thank Dr V. N. Skvortsov, Mechanical Engineering Research Institute. Russian Academy of Science for discussions of the research, and Professor A. M. Smirnitsky and Mr A. Kulagin, Mendeleev University, for consultations on interpretation of the results.

References

1. S. I. BULYICHEV and V. P. ALEKHIN, "Testing of materials by continuous intrusion of indentor" (Moscow, Mashinostrogenic, 1991), 224 p. (in Russian).
2. A. G. EVANS and E. A. CHARLES, *J. Am. Ceram. Soc.* **59** (1976) 371.
3. B. R. LAWN, A. G. EVANS and D. B. MARSHALL, *ibid.* **63** (1980) 574.
4. B. R. ANTIS, P. CHANTIKUL, B. R. LAWN and D. B. MARSHALL, *ibid.* **64** (1981) 539.
5. P. MIRAZANO and J. S. MOYA, *Ceram. Int.* **10** (1984) 147.
6. J. L. LOUBERT, J. M. GEORGES, O. MACHISHINI and J. MEILLE, *Trans. ASTMJ. Tribol.* **106** (1984) 43.
7. H. BUCKLE, in "Science of Hardness Testing and its Research Applications" (ASM, Metals Park, OH, 1971) pp. 453–94.
8. P. M. SARGENT and T. F. PAGE, *Proc. Brit. Ceram. Soc.* **26** (1978) 209.
9. A. P. TERNOVSKY, V. P. ALEKHIN, V. N. SKVORTSOV, Y. V. MALOV and A. S. ARTEMOV, in "New in the Sphere of Microhardness Testing" (Moscow, Nauka, 1974) (in Russian) pp. 71–83.
10. A. P. TERNOVSKY, V. P. ALEKHIN and S. I. BULYICHCEV, *Metallophysica* **44** (1973) 354 (in Russian).
11. I. V. GRIDNEVA, Y. V. MITMAN and V. N. TREFILOV, "Defects of Structure of Semiconductors", Proceedings of the Conference, Novosibirsk, Nauka, 1970, p. 79 (in Russian).
12. B. R. LAWN and M. S. SWAIN, *J. Mater. Sci.* **10** (1975) 113.
13. *Idem, ibid.* **10** (1975) 1049.
14. S. PALMQVIST, *Jernkontors Ann.* **5** (1957) 300.

Received 6 May 1993
and accepted 22 April 1994